Ann. Geophys., 31, 319–331, 2013
www.ann-geophys.net/31/319/2013/
doi:10.5194/angeo-31-319-2013

Annales Geophysicae
Open Access

Magnetosheath dynamic pressure enhancements: occurrence and typical properties

M. O. Archer and T. S. Horbury

Space & Atmospheric Physics Group, The Blackett Laboratory, Imperial College London, Prince Consort Road, London, SW7 2BW, UK

Correspondence to: M. O. Archer (m.archer10@imperial.ac.uk)

Received: 19 November 2012 – Revised: 5 February 2013 – Accepted: 5 February 2013 – Published: 26 February 2013

Abstract. The first comprehensive statistical study of large-amplitude (> 100 %) transient enhancements of the magnetosheath dynamic pressure reveals events of up to ∼ 15 times the ambient dynamic pressure with durations up to 3 min and an average duration of around 30 s, predominantly downstream of the quasi-parallel shock. The dynamic pressure transients are most often dominated by velocity increases along with a small fractional increase in the density, though the velocity is generally only deflected by a few degrees. Superposed wavelet transforms of the magnetic field show that, whilst most enhancements exhibit changes in the magnetosheath magnetic field, the majority are not associated with changes in the Interplanetary Magnetic Field (IMF). However, there is a minority of enhancements that do appear to be associated with solar wind discontinuities which cannot be explained simply by random events. In general, it is found that during periods of magnetosheath dynamic pressure enhancements the IMF is steadier than usual. This suggests that a stable foreshock and hence foreshock structures or processes may be important in the generation of the majority of magnetosheath dynamic pressure enhancements.

Keywords. Magnetospheric physics (Magnetosheath; Solar wind-magnetosphere interactions) – Space plasma physics (Discontinuities)

1 Introduction

The magnetosheath acts as an interface between the solar wind and the magnetopause and it is therefore important to understand how solar wind properties are modified in this region. In particular the magnetosheath pressure is relevant in terms of the position and motion of the magnetopause. Observations have shown that transient, large-amplitude enhancements in the dynamic pressure sometimes exist in the magnetosheath. Whilst some of these can be ascribed to magnetic reconnection at either the magnetopause (e.g. Paschmann et al., 1979) or current sheets (e.g. Phan et al., 2007), many such enhancements cannot. Of the latter, their kinetic energy density can far exceed that of the undisturbed solar wind, and they are often found during intervals of radial interplanetary magnetic field (Hietala et al., 2009). It is known that such enhancements in the subsolar magnetosheath can distort the magnetopause (Shue et al., 2009; Amata et al., 2011), and some have been shown to cause either localised (Hietala et al., 2012) or more global (Dmitriev and Suvorova, 2012) magnetic pulsations in the magnetosphere as well as flow enhancements in the ionosphere (Hietala et al., 2012).

Dynamic pressure enhancements have been observed in the flank (Němeček et al., 1998; Savin et al., 2011, 2012) and subsolar (Shue et al., 2009; Hietala et al., 2009, 2012; Archer et al., 2012) magnetosheath as well as near the cusps (Savin et al., 2008; Amata et al., 2011). They have dimensions ∼ 1 R_E parallel to the flow (Němeček et al., 1998; Savin et al., 2008) and exhibit much variability perpendicular to it over scales ∼ 0.2–0.5 R_E (Archer et al., 2012). The enhancements are in general due to variations in both the density and velocity (Amata et al., 2011), the former showing either increases or decreases whilst the latter generally showing increases. In roughly 70 % of the jets reported by Savin et al. (2008) in the flank magnetosheath, peaks in the density and velocity did not coincide and the peak in the dynamic pressure more often than not corresponded to the peak in density. However, Archer et al. (2012) showed dynamic

pressure pulses observed in the subsolar magnetosheath that were dominated by the velocity.

A number of different origins have been suggested for these structures. Chen et al. (1993), Lavraud et al. (2007) and Lavraud and Borovsky (2008) explained magnetosheath speeds downstream of the Earth greater than the solar wind speed as being due to magnetic forces under low-Mach-number solar wind and northward Interplanetary Magnetic Field (IMF). Hietala et al. (2009, 2012) proposed that ripples inherent to the quasi-parallel shock allow high flow speeds downstream, via the Rankine–Hugoniot relations. The bow shock changing from concave (which can occur for radial IMF (De Sterck et al., 1998; Cable et al., 2007)) to convex, allowing a high speed solar wind flow into the normal region of magnetosheath flow, has also been suggested (Shue et al., 2009). Savin et al. (2011, 2012) argue that super-magnetosonic streams in the magnetosheath can be triggered by hot flow anomalies or the interaction of the shock with rotational discontinuities, jumps in the solar wind pressure and interplanetary shocks. Similarly Němeček et al. (1998) postulated the interaction of foreshock discontinuities with the bow shock as a possible source. Archer et al. (2012) presented dynamic pressure pulses in the subsolar magnetosheath, showing that the pulses did not exist upstream of the shock (in either the pristine solar wind or foreshock) and appeared consistent with previous simulations of rotational discontinuities interacting with the shock (Lin et al., 1996a,b; Tsubouchi and Matsumoto, 2005). These simulations predict large-amplitude pulses when the local geometry of the shock changes from quasi-perpendicular to quasi-parallel or vice versa. This was also the conclusion of Dmitriev and Suvorova (2012), who observed a magnetosheath jet consistent with being generated by a discontinuity which changed the shock geometry from quasi-parallel to quasi-perpendicular.

To date, previous studies into these transient dynamic pressure enhancements have involved case studies of only a small number of events/days at a time. Whilst most studies agree that these enhancements are typically observed downstream of the quasi-parallel shock, their occurrence both spatially and under different solar wind conditions is poorly understood. It is clear that there is a large amount of variability to the properties of these structures, but the typical characteristics, their range and distributions are not known. Finally a number of origins for these enhancements have been suggested in the literature; however, which physical processes dominate and under what circumstances is yet to be determined. A comprehensive statistical study of dynamic pressure enhancements in the magnetosheath could provide insight into these topics. The first such study is presented here.

2 Method

2.1 Data

This study uses Electrostatic Analyser (McFadden et al., 2008a) and Fluxgate Magnetometer (Auster et al., 2008) data from the THEMIS (Angelopoulos, 2008) spacecraft during the 2008 dayside science phase of the mission. All magnetosheath crossings greater than an hour in duration from all five THEMIS spacecraft during June–September 2008 were identified manually (primarily using ion energy spectrograms when available, but the density, velocity and magnetic field magnitude were also used) yielding 1361 h of magnetosheath data. The positions of the spacecraft during these times are shown in Fig. 1 (left and top right) along with average magnetopause and bow shock locations (see supplementary material for the times of the magnetosheath crossings).

2.2 Magnetosheath model

It is clear that many of the crossings lie outside the average magnetosheath due to the changing solar wind conditions; therefore data were mapped onto a stationary model of the magnetosheath. One-minute-resolution OMNI solar wind data, smoothed to 20 min, was used to estimate conditions upstream at the nose of the bow shock; aberrated GSE coordinates were used to allow for the Earth's orbital motion. The location of the magnetopause was calculated using the model of Shue et al. (1998), whilst the bow shock stand-off distance was set by Farris and Russell (1994) with the bow shock shape shape given by Farris et al. (1991). Since these models are axially symmetric, the spacecraft position in the magnetosheath model can be specified by two parameters: the aberrated solar zenith angle θ (negative for the dawn magnetosheath and positive for the dusk) and the fractional magnetosheath distance F (0 at the magnetopause and 1 at the bow shock).

$$F\left(r,|\theta|\right)=\frac{r-r_{\mathrm{mp}}\left(|\theta|\right)}{r_{\mathrm{bs}}\left(|\theta|\right)-r_{\mathrm{mp}}\left(|\theta|\right)}, \tag{1}$$

where r is the radial distance of the spacecraft from the Earth and the radial distances to the model magnetopause and bow shock as a function of $|\theta|$ are $r_{\mathrm{mp}}\left(|\theta|\right)$ and $r_{\mathrm{bs}}\left(|\theta|\right)$.

Of the 1361 h worth of magnetosheath data, 1260 h had available OMNI data and these were mapped to the magnetosheath model. The coverage in this model is displayed in Fig. 1 (bottom), showing good coverage of the whole dayside magnetosheath and fairly good agreement with the model magnetopause and bow shock positions, with 1167 h for which $0 < F \leq 1$.

During all the magnetosheath crossings, magnetic field measurements and ion moments were collected at 3-s resolution. This study does not use electron plasma moments since electrons' contribution to the dynamic pressure is negligible

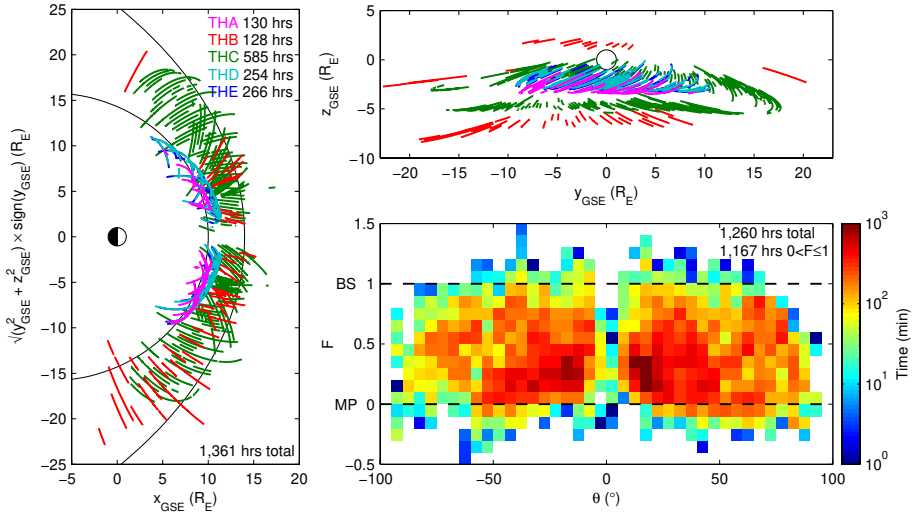

Fig. 1. Top right and left: all THEMIS magnetosheath crossings greater than an hour in duration during June–September 2008 projected radially (left) and in the GSE y–z plane (top right). The average magnetopause and bow shock locations determined by the Shue et al. (1998) and Farris et al. (1991) models, respectively, are shown as the black lines. Bottom right: coverage in the magnetosheath model, binned by aberrated solar zenith angle θ and fractional magnetosheath distance F, where the colour scale represents the amount of time in minutes spent by spacecraft in each bin. The magnetopause and bow shock are indicated by the dashed black lines.

and their thermal pressure is generally much smaller than that of ions' (e.g. Schwartz et al., 1988).

The spatial parameterisation of the magnetosheath model was checked by comparing the ratio of observed to upstream conditions with those predicted by the BATS-R-US global magnetohydrodynamic model (Powell et al., 1999). This showed very good qualitative agreement, similar to previous comparisons (Šafránková et al., 2004; Daum et al., 2008), implying good parameterisation.

2.3 Estimating θ_{Bn}

The geometry of the bow shock is important with regard to magnetosheath dynamic pressure enhancements (e.g. Hietala et al., 2009; Archer et al., 2012); therefore estimates of the magnetic field – shock normal angle θ_{Bn} are required. Since the direction of the IMF often varies over minute time scales (e.g. Vasquez et al., 2007), using 1-min-resolution OMNI data of the IMF at the bow shock nose is insufficient; hence a better estimate of the IMF associated with each magnetosheath plasma parcel is required.

In this study an automated clock angle correlation procedure was used to match up the magnetic fields observed by ACE (Smith et al., 1998) at 16-s cadence to those in the magnetosheath, the details of which can be found in Appendix A. This technique resulted in estimates of the IMF 70 % of the time.

Estimates of the shock normal are also needed. The semi-empirical magnetosheath model of Kallio and Koskinen (2000) was used to trace streamlines back to the model shock, since it is computationally inexpensive and provides streamlines consistent with the magnetopause and bow shock models used (the forms of these boundaries are an input to the model). This provides a shock normal at all times the spacecraft were in the model magnetosheath, i.e. $0 < F \leq 1$. For the majority of the surveyed magnetosheath, the sensitivity of the bow shock normals to different streamline models was small, of the order of a few degrees. Therefore the resulting shock normals are generally reliable and can be combined with the lagged ACE data to give estimates of the magnetosheath θ_{Bn}.

2.4 Dynamic pressure enhancements

In order to identify dynamic pressure enhancements in the magnetosheath, an ambient dynamic pressure must first be defined. This was set equal to a 20-min running average of the magnetosheath dynamic pressure, a time scale much longer than the typical recurrence of dynamic pressure pulses (Archer et al., 2012). The fractional change in the dynamic pressure was then calculated and a threshold implemented with enhancements defined as

$$\frac{\delta P_{\mathrm{dyn}}}{\langle P_{\mathrm{dyn}} \rangle} > 1, \tag{2}$$

where angular brackets denote the time averaging procedure. No such enhancements were present in the 1-min OMNI data or 3-s ion data from WIND's 3-D Plasma and Energetic Particle Investigation (Lin et al., 1995). Therefore no identified magnetosheath dynamic pressure enhancements originated entirely in the solar wind.

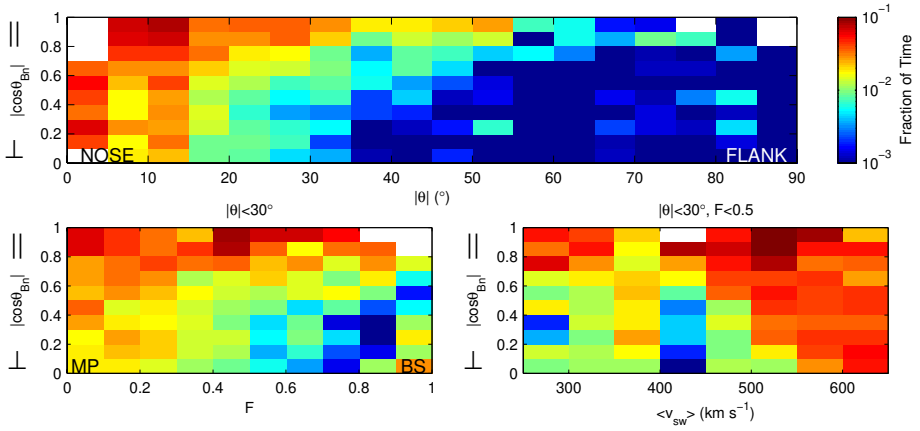

Fig. 2. Bivariate histograms where the logarithmic colour scale represents the fraction of the time that dynamic pressure enhancements ($\delta P_{\mathrm{dyn}}/\langle P_{\mathrm{dyn}}\rangle > 1$) are observed. All panels show the absolute cosine of the magnetic field – shock normal angle $|\cos\theta_{Bn}|$ along the vertical. Across the horizontal (top) are the aberrated solar zenith angle $|\theta|$; bottom left: magnetosheath fractional distance F shown for the subsolar ($|\theta| < 30°$) case; and bottom right: solar wind speed for the subsolar inner ($|\theta| < 30°$ and $F < 0.5$) magnetosheath. White areas indicate poor coverage from the magnetosheath survey.

3 Occurrence

Overall dynamic pressure enhancements constituted $\sim 2\,\%$ of the entire magnetosheath data set. In order to understand their occurrence, the magnetosheath data were binned by a number of different variables and the fraction of data points satisfying Eq. (2) in each bin calculated. Any bin with less than 25-min worth of coverage was rejected. Figure 2 shows the results of this analysis.

The occurrence of enhancements has a strong dependence on θ_{Bn}, being more frequent ($\sim 3\,\%$ of the time) when downstream of the quasi-parallel shock compared to the highly perpendicular case ($\sim 0.5\,\%$), consistent with Němeček et al. (2001), Hietala et al. (2009, 2012) and Archer et al. (2012). The top panel in Fig. 2 also shows the variation with aberrated solar zenith angle θ. As no strong dawn–dusk asymmetry in the occurrence of pulses was observed, the absolute value is used. It is clear that dynamic pressure enhancements are more frequent behind the quasi-parallel shock for all zenith angles. Enhancements also become more common as $|\theta|$ decreases; this is the case irrespective of geometry but is more distinct behind the quasi-perpendicular shock. However, this behaviour may be an effect of the ambient plasma velocity, which is faster in the flanks than the subsolar magnetosheath, since a larger velocity increase would be required to produce a given fractional change $\delta P_{\mathrm{dyn}}/\langle P_{\mathrm{dyn}}\rangle$.

The enhancement occurrence as a function of fractional magnetosheath distance F for the subsolar ($|\theta| < 30°$) magnetosheath is shown in Fig. 2 (bottom left). This reveals that the origin of the enhancements behind the quasi-parallel and quasi-perpendicular bow shocks appear to be different. Enhancements downstream of the quasi-parallel shock appear to be generated at the shock itself, since there is no obvious trend in their occurrence with F. This is also the case in the flanks (not shown). In contrast the frequency of enhancements increases near to the magnetopause behind the quasi-perpendicular shock (though the trend is weaker in the case of the flanks). This could imply that they are associated with the magnetopause.

Finally, the variation with solar wind speed for the subsolar inner magnetosheath ($|\theta| < 30°$ and $F < 0.5$) is shown in Fig. 2 (bottom right) with an increase in the occurrence of enhancements with solar wind speed seen, especially behind the quasi-perpendicular shock. No such relationship could be determined for the outer subsolar or either flank cases since data coverage was insufficient to select by F. Note that, in the inner, quasi-perpendicular magnetosheath, identified enhancements may be due to reconnection at the magnetopause or acceleration near the plasma depletion layer; hence the reason behind the trend with solar wind speed is unclear.

Similar analysis (not shown here) demonstrated that the occurrence of dynamic pressure enhancements in the magnetosheath showed no clear dependence on the IMF clock angle, solar wind plasma β or Mach number. Therefore it is unlikely that the enhancements can be explained by the "magnetic slingshot" effects described by Chen et al. (1993), Lavraud et al. (2007) and Lavraud and Borovsky (2008), which come into play predominantly downstream of the Earth (this study looks into the dayside only) under low-Mach-number solar wind and northward IMF. Using 200 % enhancements rather than 100 % does not make a qualitative difference to the results presented here. These are in agreement with the statistical study of magnetosheath ion flux variations by Němeček et al. (2001), which showed an increase in the relative standard deviation toward the magnetopause, as the IMF cone angle decreased and solar wind velocity increased respectively. However, it has been shown here that the behaviour with position in the magnetosheath and the

solar wind speed is very different depending on the magnetosheath θ_{Bn}; hence this is the main controlling parameter in the occurrence of dynamic pressure enhancements.

4 Properties

Dynamic pressure enhancements of up to ~ 15 times the background in amplitude were observed by THEMIS. The dynamic pressure can vary due to either density or velocity variations or both. This section addresses which of these is dominant.

4.1 Parameter space

The same technique as that of Archer et al. (2012) was employed, whereby both terms in the dynamic pressure are expressed as being equal to a background value (given by a 20-min running average) plus some deviation, i.e.

$$\rho = \langle\rho\rangle + \delta\rho \tag{3a}$$

$$v^2 = \left\langle v^2 \right\rangle + \delta\left(v^2\right), \tag{3b}$$

where ρ is the density and v the flow speed. Since the averaging period is much greater than the typical recurrence of dynamic pressure enhancements, and therefore the correlation scale, the approximation

$$\left\langle \rho v^2 \right\rangle \simeq \langle\rho\rangle \left\langle v^2 \right\rangle \tag{4}$$

can be used; the difference of these two quantities was less than 10 % for 99 % of the magnetosheath survey. Combining Eqs. (3a), (3b) and (4) it is possible to consider the relative contributions of density and velocity variations to the amplitude of the dynamic pressure:

$$\delta P_{\mathrm{dyn}} = \delta\left(\rho v^2\right) \tag{5a}$$

$$= \rho v^2 - \left\langle \rho v^2 \right\rangle \tag{5b}$$

$$\simeq \rho v^2 - \langle\rho\rangle \left\langle v^2 \right\rangle \tag{5c}$$

$$\simeq \delta\rho \left\langle v^2 \right\rangle + \langle\rho\rangle\, \delta\left(v^2\right) + \delta\rho\delta\left(v^2\right) \tag{5d}$$

$$1 \simeq \frac{\delta\rho \left\langle v^2 \right\rangle}{\delta P_{\mathrm{dyn}}} + \frac{\langle\rho\rangle\, \delta\left(v^2\right)}{\delta P_{\mathrm{dyn}}} + \frac{\delta\rho\delta\left(v^2\right)}{\delta P_{\mathrm{dyn}}} \tag{5e}$$

$$\simeq \frac{\delta\rho/\langle\rho\rangle}{\delta P_{\mathrm{dyn}}/\left\langle P_{\mathrm{dyn}}\right\rangle} + \frac{\delta\left(v^2\right)/\left\langle v^2\right\rangle}{\delta P_{\mathrm{dyn}}/\left\langle P_{\mathrm{dyn}}\right\rangle} + \frac{\left(\delta\rho/\langle\rho\rangle\right)\left(\delta\left(v^2\right)/\left\langle v^2\right\rangle\right)}{\delta P_{\mathrm{dyn}}/\left\langle P_{\mathrm{dyn}}\right\rangle}. \tag{5f}$$

The first term on the right-hand side of Eq. (5f) (here referred to as the density term) refers to the contribution to the dynamic pressure due to density variations, the second term is due to velocity changes (velocity term) and the third (correlation term) relates to changes in both.

The relative contributions of density and velocity variations to the dynamic pressure transients can then be represented in the density–velocity term parameter space. Since its construction makes no assumption as to the sign or magnitude of the change in dynamic pressure, it is completely general. In this study, however, only data satisfying Eq. (2) is used; hence only a subset of the full parameter space is investigated.

4.2 Distribution

Figure 3a shows the distribution of enhancements in the density–velocity term parameter space. The enhancement amplitude $\delta P_{\mathrm{dyn}}/\left\langle P_{\mathrm{dyn}}\right\rangle$ is a function of the position in this parameter space, contours of which are shown as the black dashed lines. The distribution is fairly continuous; however it is possible to divide it up into three main regions:

1. **Density decreases**: 18 % of enhancements show a decrease in density but increase in velocity.
2. **Density increases**: 82 % contain increases in both density and velocity. The largest amplitude enhancements are in this category.
3. **Velocity decreases**: Enhancements where the velocity decreases (by a few percent) but the density increases (at least doubles) are extremely rare. These could be related to the "embedded plasmoids" of Karlsson et al. (2012); however no further discussion shall be made here.

Figure 3a shows that the dynamic pressure increase of the transients is typically dominated by the velocity, with the peak in the distribution (shown by the black dot) being close to a density term of zero. This is likely because the velocity in the dynamic pressure is squared: for a given fractional increase in velocity, the fractional increase in the velocity squared will be greater. Indeed modelling the fluctuations $\delta v/\langle v\rangle$ and $\delta\rho/\langle\rho\rangle$ as normally distributed random variables (with zero mean and a number of different standard deviations) yields fairly similar parameter space distributions and roughly the same partition between density-increase and -decrease events. However, it is of course important to understand the physical processes which generate such large fluctuations in these properties.

4.3 Typical properties

In order to ascertain for the first time the typical properties of the enhancements, the means of various quantities in each parameter space bin were calculated. These results are shown in Fig. 3b–m, where bins with fewer than 4 data points have been neglected.

4.3.1 Density decreases: Flux Transfer Events

Enhancements with density decreases seem to generally be observed at small θ and F (panels b–c) and therefore could

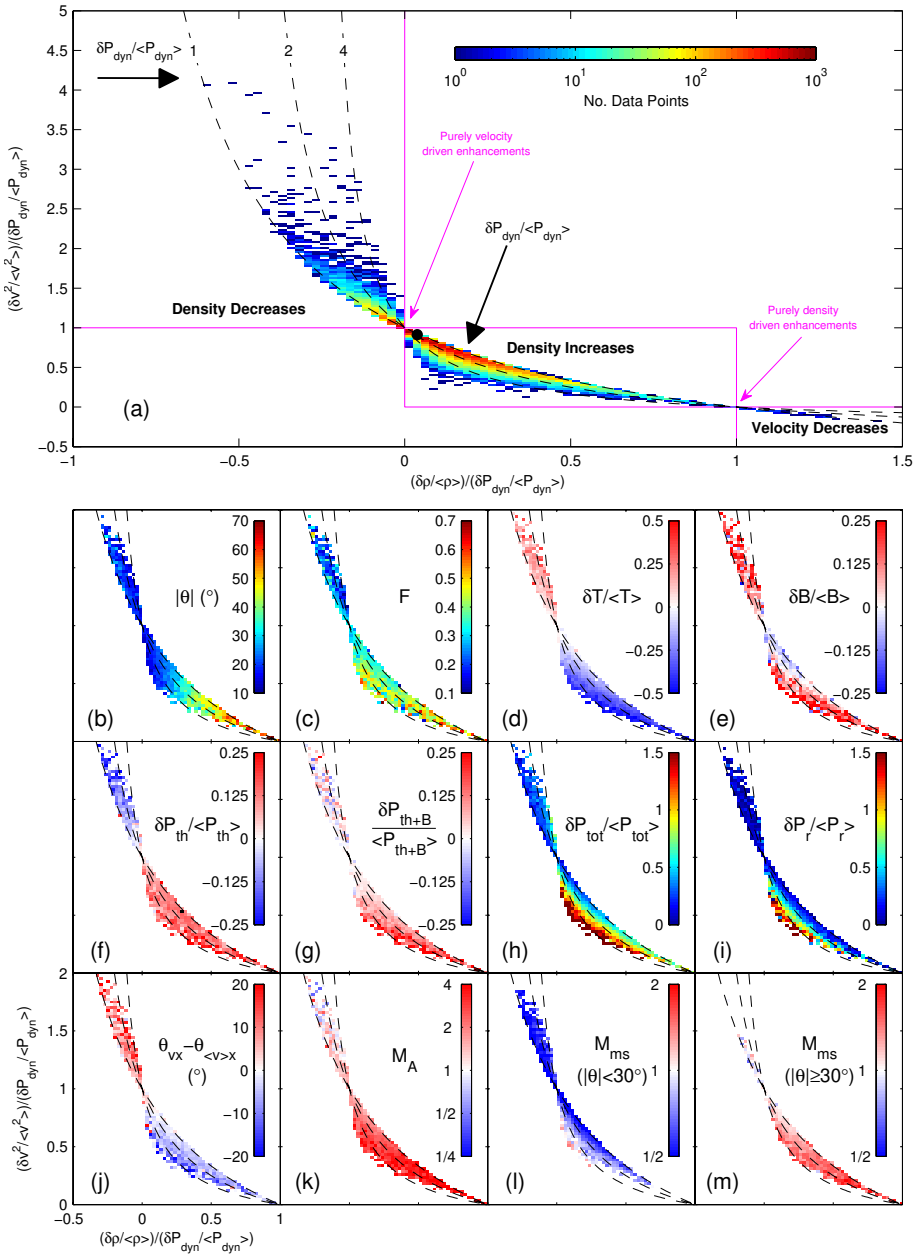

Fig. 3. **(a)** Distribution of dynamic pressure enhancements in the density–velocity term parameter space where the colour scale is the number of data points in each bin. The black dot marks the maximum of the distribution. Three different regions are indicated by the magenta lines. Contours of $\delta P_{\mathrm{dyn}}/\langle P_{\mathrm{dyn}}\rangle$ are given by the black dashed lines, with the black arrows specifying the direction of increasing $\delta P_{\mathrm{dyn}}/\langle P_{\mathrm{dyn}}\rangle$ in the different regions. **(b)**–**(m)** Means in each parameter space bin of the **(b)** aberrated solar zenith angle; **(c)** fractional magnetopause distance; **(d)** fractional temperature change; **(e)** fractional magnetic field strength change; **(f)** fractional ion thermal pressure change; **(g)** fractional change in ion thermal and magnetic pressures; **(h)** fractional total pressure change; **(i)** fractional radially inward pressure change; **(j)** change in the velocity cone angle; **(k)** Alfvénic Mach number; and magnetosonic mach numbers for both the **(l)** subsolar and **(m)** flank cases.

be associated with the subsolar magnetopause. Flux Transfer Events (FTEs), thought to be spatially and temporally limited reconnection events occurring at the dayside magnetopause (Russell and Elphic, 1978), are thus a likely candidate. The signatures of FTEs observed in the magnetosheath include a decrease in the density, increase in temperature, increase in the magnetic field strength and sometimes an enhancement of flow speed (e.g. Le et al., 1999). Indeed Fig. 3d–e demonstrates that the density decreases exhibit all of these properties. Furthermore the velocity, whilst enhanced, is around the local Alfvén speed (panel k) and highly deflected but

generally to increasing cone angle (panel j), which again are consistent with a FTE origin.

FTEs would be expected at the subsolar magnetopause under southward IMF. To test this, the mean IMF clock angle α and acute cone angle θ_{Bx} were calculated in the parameter space bins from the lagged ACE data. Figure 4 shows these results, demonstrating that the density decreases typically occur under southward and high-cone-angle IMF. In contrast, the density increases are generally observed at smaller cone angles, i.e. behind the quasi-parallel shock. Therefore apart from the bipolar magnetic field signature, which cannot be extracted from this analysis, the average behaviour of the density decreases has been shown to be consistent with FTEs.

4.3.2 Density increases

In Sect. 4.3.1 it was established that enhancements with density increases tend to occur downstream of the quasi-parallel shock, but their typical properties are still unclear. Figure 3b shows that the more density driven enhancements tend to occur in the flanks. This seems consistent with previous case studies where subsolar enhancements have been reported as being generally dominated by velocity enhancements (Archer et al., 2012), whereas those in the flank show relatively more density driven enhancements (Savin et al., 2008; Amata et al., 2011). The latter of these could be density pileups as previously reported by Savin et al. (2008). These might be expected more often in the flanks as the streamlines followed back to the shock are longer than in the subsolar case, meaning more ambient plasma could be compressed by a velocity enhancement that originated at the shock.

Previous studies (Hietala et al., 2009, 2012; Savin et al., 2011, 2012) have focussed on whether the velocity becomes supermagnetosonic in these transient structures. Figure 3k–m shows the Alfvénic and magnetosonic Mach numbers. The density increases are generally highly super-Alfvénic throughout the magnetosheath and hence cannot be explained by reconnection since the Walén relation (e.g. Walén, 1944; Gosling et al., 2005) is not obeyed. The magnetosonic Mach number shows different behaviours in the subsolar ($|\theta| < 30°$) and flank ($|\theta| \geq 30°$) regions. In the latter, since the ambient flow is faster, typically all dynamic pressure enhancements are supermagnetosonic, whereas in the subsolar magnetosheath only enhancements with amplitudes $\delta P_{\rm dyn}/\langle P_{\rm dyn}\rangle \gtrsim 4$ typically are. Therefore, the enhancements' magnetosonic Mach number is highly dependent on the position in the magnetosheath, and thus this quantity may not be particularly helpful in identifying these structures.

The velocity is typically deflected to decreasing cone angle θ_{vx} (panel j), i.e. towards the Sun–Earth line, consistent with the solar wind flow not being fully shocked, e.g. via bow shock ripples (Hietala et al., 2009, 2012). However, the size of this deflection is much smaller than would be expected from these theories at typically only a few degrees.

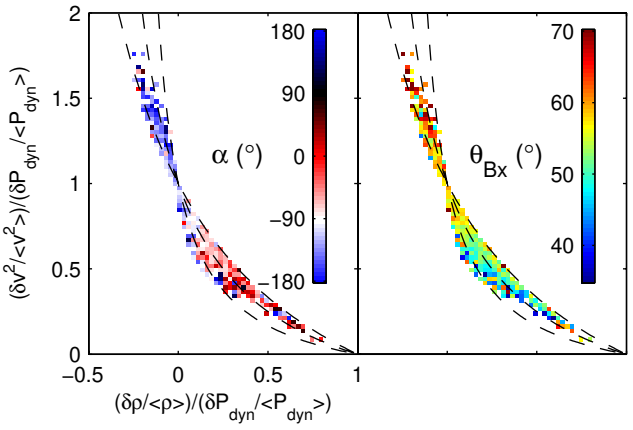

Fig. 4. Variation of the IMF clock angle α (left) and acute cone angle θ_{Bx} (right), for dynamic pressure enhancements, in the same format as Fig. 3.

The density increases are colder than their surroundings (Fig. 3d), consistent with Savin et al. (2008) and Archer et al. (2012), though the ion thermal pressure $P_{\rm th} = nk_BT$ shows a small increase (panel f); overall the density variations dominate the thermal pressure in these structures. The majority of the density increases have a very small decrease in the magnetic field strength (panel e). Magnetic depressions are expected from simulations of rotational discontinuities interacting with the bow shock (Lin et al., 1996a,b; Tsubouchi and Matsumoto, 2005), though the observed depression here is much weaker than in the simulations.

There is a transition in the magnetic field behaviour whereby the field strength increases for enhancements with $\delta\rho/\langle\rho\rangle \gtrsim 0.4$. Whilst it is not clear what causes this, it may be an effect of simple compression of the plasma. The magnetic field increases affect the thermal plus magnetic pressure $P_{\rm th+B} = P_{\rm th} + P_B$, deviating from approximate pressure balance (panel g).

The dynamic pressure enhancements significantly increase the total (dynamic + ion thermal + magnetic) pressure, up to ~ 2 times the ambient (panel h). In terms of the potential magnetospheric impact, the change in the radially inwards pressure was calculated (panel i):

$$P_{\rm r} = \rho v_{\rm r}^2 \times \mathrm{sign}\,(v_{\rm r}) + P_{\rm th} + P_B, \quad (6)$$

where $v_{\rm r} = -\boldsymbol{v}\cdot\boldsymbol{r}/r$ is the component of the ion velocity directed radially towards the Earth. For $\delta P_{\rm dyn}/\langle P_{\rm dyn}\rangle \gtrsim 2$ this shows increases of $\sim 50\,\%$, which could have significant effects on the magnetopause and within the magnetosphere. These enhancements occur in the magnetosheath $\sim 0.3\,\%$ of the time.

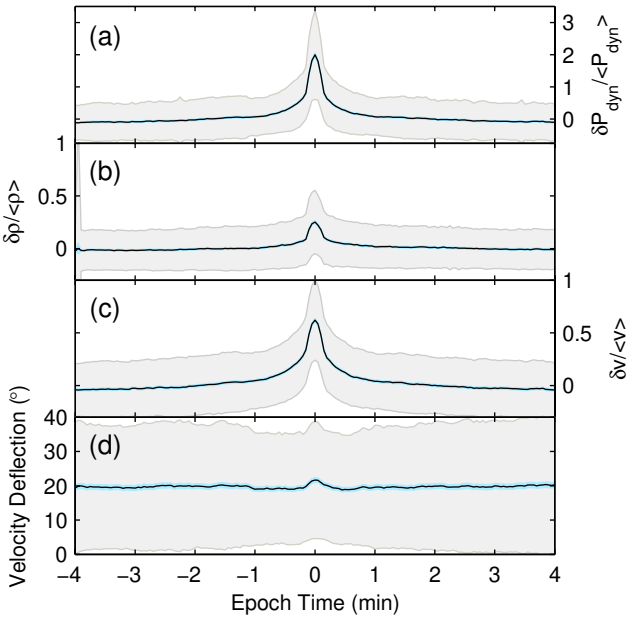

Fig. 5. Superposed epoch analysis of dynamic pressure enhancements. **(a)** Fractional change in dynamic pressure, **(b)** fractional change in density, **(c)** fractional change in flow speed, **(d)** angular deflection of the velocity. Solid black lines represent the mean values, and corresponding standard deviations and 95 % confidence intervals are shown in grey and blue, respectively.

5 Superposed epoch analysis

To aid the identification of the dominant mechanism responsible for generating dynamic pressure enhancements, a superposed epoch analysis (SEA) was performed on all events with $\delta P_{\mathrm{dyn}}/\langle P_{\mathrm{dyn}}\rangle > 1$. The procedure identified 2617 events from the 5-data-point-smoothed spacecraft time series; 25 % of which had amplitudes greater than 2. The durations in the spacecraft frame were 12–201 s (mean 34 s), consistent with previous results (e.g. Němeček et al., 1998; Savin et al., 2008). Results from the SEA are shown in Fig. 5 where the mean is shown; the median yielded qualitatively similar results. While this procedure averages over all enhancements of all types, it is dominated by the more common velocity-driven, density-increase events.

5.1 Results

The SEA produced a dynamic pressure enhancement whose position in the density–velocity term parameter space is not dissimilar to the peak of the distribution (the black dot in Fig. 3a). While the standard deviations are large (as expected given the distribution) they are fairly constant in time; thus due to the large number of events the confidence interval in the mean is small. The results of the SEA for other quantities were found to be in agreement with the typical properties identified in Sect. 4.

In addition the analysis produced results on the total angular deflection of the velocity increases inside the dynamic pressure transients. SEA of the angle between the observed and smoothed velocity vectors is shown in Fig. 5d. This is necessarily a positive quantity and therefore does not average to zero outside of the dynamic pressure transient. Indeed the ambient value, which signifies the typical background variability of the velocity direction, is rather large at around 20°. This is likely due to events being more common in the quasi-parallel magnetosheath, which is generally more turbulent (Lucek et al., 2005). The deflection angle inside the dynamic pressure transient is only a few degrees larger than this ambient value; therefore the change in direction of the velocity of the enhancements is not much more than the natural variability. Again the standard deviation, whilst large, is similar both inside and outside of the transient.

Hietala et al. (2009, 2012) proposed that dynamic pressure enhancements could be explained by ripples in the bow shock allowing fast streams of plasma downstream via the Rankine–Hugoniot relations, necessarily deflecting the plasma flow significantly. Since SEA shows that the flow is greatly enhanced but not highly deflected, these ideas cannot explain the typical behaviour of magnetosheath dynamic pressure enhancements. Nonetheless, the analysis does not preclude that some enhancements may originate from such ripples.

5.1.1 Association with discontinuities?

A number of proposed mechanisms for the generation of magnetosheath dynamic pressure enhancements require a solar wind discontinuity interacting with the bow shock in some way (e.g. Lin et al., 1996a,b; Savin et al., 2011, 2012). Are enhancements typically associated with discontinuities?

Identifying discontinuities is often difficult, especially in the magnetosheath, and a number of different selection criteria with different thresholds have previously been developed (e.g. Smith, 1973; Vasquez et al., 2007). These methods attempt to identify the magnetic fields either side of the discontinuity. Since the proposed mechanisms for the enhancements generally have no preferred magnetic orientation other than one side being quasi-parallel, SEA of the individual components of the magnetic field would not be expected to produce a signal. However, if one is simply interested in whether the magnetic field changes at all, then the wavelet transform can provide insight: the wavelet transform of a discontinuity (or jump) in a time series is seen as an increase in power at all frequencies, limited in time by the wavelet's cone of influence centred on the discontinuity.

The Morlet wavelet transform of the three GSE magnetic field components were calculated, as per Torrence and Compo (1998), for both the THEMIS and ACE data. In order to exclude any edge effects from the analysis, only events with a full (i.e. no data gaps) 10-min worth of magnetic field data either side were used, resulting in 1707 enhancements

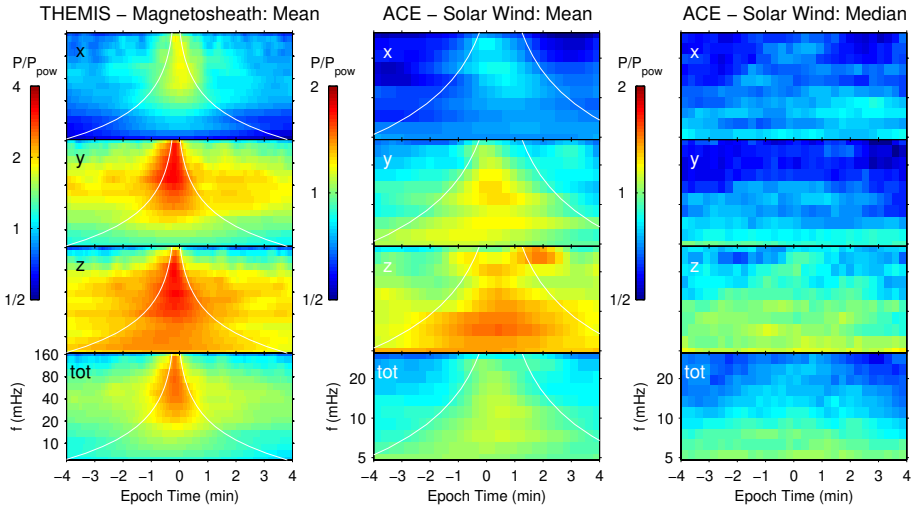

Fig. 6. Left: mean of the superposed wavelet power of the magnetosheath magnetic field. The median was similar. Middle and right: mean (middle) and median (right) of the superposed wavelet power of the solar wind magnetic field. The four panels show the power in the three GSE components of the magnetic field as well as the total. The respective mean background power law spectra P_{pow} over all three components have been removed for clarity, with a similar procedure performed for the total power also. White lines indicate the Morlet wavelet cones of influence.

from THEMIS and 1187 from ACE. Superposed epoch analysis was performed on the wavelet power P for each component of the magnetic field as well as the total power in all components, shown in Fig. 6 where the background (at ± 4 min epoch time) power law spectrum P_{pow} has been subtracted for clarity. The results of the analysis were unaffected by only selecting those events with both THEMIS and ACE wavelet transforms.

In the magnetosheath the wavelet power in all three components shows a significant increase at all frequencies around the events, though this is smallest in the x-component. The increases are fairly well described temporally by the Morlet wavelet's cone of influence centred on the feature (shown by the white lines in Fig. 6), suggesting a sharp change in the field. The same feature is observed when the median is used in the analysis; hence these results are not simply due to highly skewed distributions. A null analysis was also performed, using the same number of events but picked entirely at random, which yielded no features. Figure 7 shows that the background total wavelet power is larger for the dynamic pressure enhancements than would be expected by chance: this is probably because events tend to occur in the quasi-parallel magnetosheath, which contains larger fluctuations in the magnetic field (Luhmann et al., 1986). It has been found here that dynamic pressure enhancements typically have associated sharp changes in the magnetosheath magnetic field which may be discontinuities.

To ascertain whether these changes in the magnetosheath field typically originate in the solar wind, similar analysis was performed on lagged ACE data for 1187 events with the results shown in Fig. 6 (middle and right). In the mean

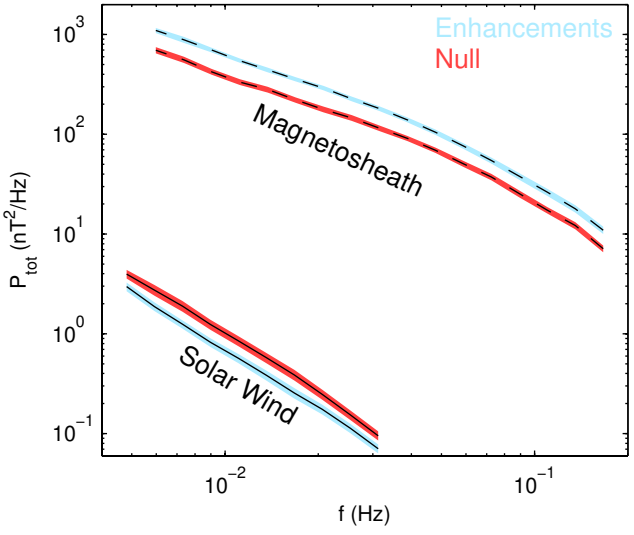

Fig. 7. Mean background superposed wavelet power spectra in the magnetosheath (dashed lines) and solar wind (solid lines) are shown, along with corresponding 95 % confidence intervals (coloured regions) for both the dynamic pressure enhancements (blue) and null (red) events.

(middle), a similar discontinuity-like increase in the wavelet power is seen, largest in the z-component. However the median (right) showed no such feature (neither did the null analysis). This means that the increase exhibited in the mean is due to the distribution becoming more skewed than the background distribution. Therefore, the majority of magnetosheath dynamic pressure enhancements do not show an increase in wavelet power of the solar wind magnetic field and

hence are not associated with changes in the IMF. Nonetheless, there is a minority of enhancements that do appear to be associated with solar wind discontinuities which cannot be explained by chance, though quantifying this fraction is difficult.

The mean background total wavelet power in the solar wind, shown in Fig. 7, is typically smaller for the enhancements than that for the null events. Thus during periods of magnetosheath dynamic pressure enhancements, the IMF is generally steadier than usual. Since the enhancements are predominantly found downstream of the quasi-parallel shock, this suggests that a stable foreshock is important in the generation of the majority of magnetosheath dynamic pressure enhancements.

6 Discussion and conclusions

In this paper, the first comprehensive statistical study of large-amplitude, transient enhancements of the magnetosheath dynamic pressure has been presented. Enhancements of up to ~ 15 times the ambient dynamic pressure in amplitude were observed, similar to the observations of Archer et al. (2012), with durations 10 s to 3 min, consistent with previous studies (e.g. Němeček et al., 1998; Savin et al., 2008). The dynamic pressure transients are most often dominated by velocity increases and the density can either increase or decrease, broadly separating the enhancements into two different regimes.

Those with density decreases are much less frequent (18 % of all enhancements) and are typically consistent with FTEs at the subsolar magnetopause under southward, high-cone-angle IMF. On the other hand, previous case studies have identified dynamic pressure enhancements in the magnetosheath containing depressions in the density which could not be attributed to reconnection (Shue et al., 2009; Hietala et al., 2009). It therefore appears that such events are not very common.

In contrast, enhancements containing increases in the density are by far the most common, though the fractional increase in density is usually small. They are characterised by a decrease in the ion temperature but slight increase in thermal pressure and a small velocity deflection to smaller cone angle. On average the deflection is only a few degrees; consequently the large increases in flow speed cannot typically be explained by the bow shock ripple ideas proposed by Hietala et al. (2009, 2012). The flow is also highly super-Alfvénic and hence cannot be attributed to reconnection. However, the typical properties presented cannot unambiguously identify the predominant origin of the enhancements from those previously proposed.

The dynamic pressure enhancements with density increases predominantly occur under low-cone-angle IMF, in contrast to those with density decreases. In general, enhancements of both types are most frequent throughout the quasi-parallel magnetosheath and are therefore likely to be generated at or near the shock, in agreement with previous results (e.g. Němeček et al., 1998; Hietala et al., 2009; Archer et al., 2012). On the other hand, those downstream of the quasi-perpendicular shock are most often observed close to the magnetopause. These include the previously identified FTEs and could also consist of jets/pulses deflected or reflected by the magnetopause, as previously shown by Amata et al. (2011), or accelerated flows near the plasma depletion layer. It is also found that enhancements are more frequent with decreasing zenith angle and increasing solar wind speed, though no clear dependence on IMF clock angle, solar wind plasma β or Mach number could be found. Hence it is unlikely that the enhancements reported here can be explained by "magnetic slingshot" effects (Chen et al., 1993; Lavraud et al., 2007; Lavraud and Borovsky, 2008), which predominantly occur dowstream of the Earth under low-Mach-number solar wind and northward IMF. The reasons for the trends presented here are unclear at present and require further investigation.

Solar wind discontinuities feature in a number of previously proposed origins of magnetosheath dynamic pressure enhancements (e.g. Lin et al., 1996a,b; Savin et al., 2011, 2012). However, it seems that, whilst some (more than can be explained by chance) are associated with changes in the IMF, these are in the minority. In fact during periods of magnetosheath dynamic pressure enhancements, the IMF is typically steadier than usual. Němeček et al. (1998) postulated that foreshock discontinuities could interact with the shock in an analogous way to the simulations of those originating in the solar wind (e.g. Lin et al., 1996a,b). Such foreshock discontinuities/structures could be the origin of the observed sharp changes in the magnetosheath magnetic field. It is likely that such structures require a stable foreshock in order to develop and therefore a steady quasi-radial IMF. Therefore, it might be that foreshock structures/processes are important in the generation of the majority of magnetosheath dynamic pressure enhancements. Hybrid or kinetic simulations could provide insight into the downstream signatures of foreshock structures and how they compare with the typical properties of the dynamic pressure enhancements reported here. Furthermore, multipoint observations immediately upstream and downstream of the quasi-parallel shock may also aid in understanding the physical processes resulting in these enhancements in the magnetosheath. Since the effective pressure on the magnetopause is typically significantly enhanced by these structures and it is known that they can have magnetospheric effects (e.g. Shue et al., 2009; Amata et al., 2011; Hietala et al., 2012), furthering our comprehension of the processes which generate these enhancements is important.

Appendix A

Clock angle correlation procedure

The following details the automated clock angle correlation procedure used to match up ACE observations of the IMF with the magnetic field measured by THEMIS in the magnetosheath. For each THEMIS magnetosheath crossing,

1. the lag times to the bow shock nose for ACE from the OMNI database were looked up and averaged for the entire crossing. If none were available, then the OMNI lag time was interpolated to the centre of the interval. The resulting lag time is denoted by t_1.

2. the THEMIS magnetometer data was smoothed by a 1-min running average to filter out turbulence and high-frequency waves. This data was then interpolated onto the same resolution as ACE, i.e. 16 s. The ACE data for the entire magnetosheath crossing, lagged by t_1 and buffered either side by 60-min worth of data, was similarly smoothed.

3. the complex exponential of the GSE clock angle $z = \exp(i\alpha)$, where $\alpha = \arctan\left(B_y/B_z\right)$, was calculated for both the smoothed THEMIS and ACE data yielding z_{msh} and z_{sw}, respectively. The mean of z_{msh} was removed from both data sets and these were cross-correlated. The lag corresponding to the peak in the real part of the cross-correlation function was extracted as t_2, a better estimate of the overall lag time for the magnetosheath crossing. This was limited to within 30 min of t_1.

4. the magnetosheath crossing was split into intervals of 30-min duration, stepped on by 5 min at a time. For each interval,

   (a) z_{msh} was calculated and, after subtracting the mean value, a 30-min Hann window applied. z_{sw} was also calculated for the interval (buffered either side by 40 min) using a lag of t_2, with the mean of z_{msh} also subtracted. This was then cross-correlated with the windowed magnetosheath data.

   (b) all positive peaks in the real part of the cross-correlation function were identified (limited to within 20 min of t_2). Of those peaks, only those at least half the height of the tallest were considered.

   (c) if only one peak remained, then the lag associated with this peak was used. Otherwise, if previous windows had yielded a good (> 0.75) correlation coefficient (see 4d) then the peak closest to the mean of these lag times was chosen. If no previous windows had good correlation coefficients then the peak closest to a lag of t_2 was picked. t_3 denotes the chosen lag time for each interval.

   (d) the Hann-weighted correlation coefficient of z_{msh} and z_{sw}, the latter now lagged by t_3, was calculated.

5. all lags t_3 from intervals where the correlation coefficient was greater than 0.75 were accepted, with the lags interpolated for all other intervals. For any intervals before the first or after the last accepted lags, the nearest accepted lag was used. If no intervals yielded an accepted lag then all were set to t_2. This final set of lags for each interval is denoted t_4.

6. the correlation coefficients were recalculated, using the final lags t_4, as well as the Hann-weighted root mean squared deviation (RMSD) in the clock angles. These lags were accepted if their correlation coefficient > 0.75 or RMSD $< 30°$.

Table A1. Results of clock angle correlation procedure.

Corr. Coef.	RMSD	Intervals
> 0.75	$< 30°$	24 %
> 0.75	$\geq 30°$	1 %
≤ 0.75	$< 30°$	45 %
≤ 0.75	$\geq 30°$	30 %

Table A1 shows the results of this procedure for all spacecraft over all magnetosheath crossings, for which only 30 % did not produce a good lag. It was found that this percentage showed no strong dependence on θ, F, IMF cone angle or ACE's distance from the Sun–Earth line. In fact these results agree extremely well with the statistical survey of solar wind (measured by WIND) and magnetosheath (measured by Geotail and Interball-Tail) clock angles of Coleman (2005), which found about 30 % of data points exhibited perfect draping within $\pm 10°$, 70 % were within 30° and that the differences were not, in general, well ordered in any systematic fashion that could be accounted for by hydrodynamic draping.

Supplementary material related to this article is available online at: http://www.ann-geophys.net/31/319/2013/angeo-31-319-2013-supplement.zip.

Acknowledgements. We thank J. P. Eastwood and the reviewers for their helpful comments. This research at Imperial College London was funded by STFC. We acknowledge NASA contract NAS5-02099 and V. Angelopoulos for use of data from the THEMIS Mission – specifically C. W. Carlson and J. P. McFadden for use of ESA data and K. H. Glassmeier, U. Auster and W. Baumjohann for the use of FGM data provided under the lead of the Technical University of Braunschweig and with financial support through the German Ministry for Economy and Technology and the German Center

for Aviation and Space (DLR) under contract 50 OC 0302 – and N. Ness via the ACE Science Center for ACE magnetic field data. The OMNI data was obtained from the NASA/GSFC OMNIWeb interface at http://omniweb.gsfc.nasa.gov.

Topical Editor L. Blomberg thanks D. L. Turner and two anonymous referees for their help in evaluating this paper.

References

Amata, E., Savin, S. P., Ambrosino, D., Bogdanova, Y. V., Marcucci, M. F., Romanov, S., and Skalsky, A.: High kinetic energy density jets in the Earth's magnetosheath: a case study, Planet. Space Sci., 59, 482–494, doi:10.1016/j.pss.2010.07.021, 2011.

Angelopoulos, V.: The THEMIS mission, Space Sci. Rev., 141, 5–34, doi:10.1007/s11214-008-9336-1, 2008.

Archer, M. O., Horbury, T. S., and Eastwood, J. P.: Magnetosheath pressure pulses: generation downstream of the bow shock from solar wind discontinuities, J. Geophys. Res., 117, A05228, doi:10.1029/2011JA017468, 2012.

Auster, H. U., Glassmeier, K. H., Magnes, W., Aydogar, O., Baumjohann, W., Constantinescu, D., Fischer, D., Fornacon, K. H., Georgescu, E., Harvey, P., Hillenmaier, O., Kroth, R., Ludlam, M., Narita, Y., Nakamura, R., Okrafka, K., Plaschke, F., Richter, I., Schwarzl, H., Stoll, B., Valavanoglou, A., and Wiedemann, M.: The THEMIS Fluxgate Magnetometer, Space Sci. Rev., 141, 235–264, doi:10.1007/s11214-008-9365-9, 2008.

Cable, S., Lin, Y., and Holloway, J. L.: Intermediate shocks in three-dimensional magnetohydrodynamic bow-shock flows with multiple interacting shock fronts, J. Geophys. Res., 112, A09202, doi:10.1029/2007JA012419, 2007.

Chen, S.-H., Kivelson, M. G., Gosling, J. T., Walker, R. J., and Lazarus, A. J.: Anomalous aspects of magnetosheath flow and of the shape and oscillations of the magnetopause during an interval of strongly northward interplanetary magnetic field, J. Geophys. Res., 98, 5727–5742, doi:10.1029/92JA02263, 1993.

Coleman, I. J.: A multi-spacecraft survey of magnetic field line draping in the dayside magnetosheath, Ann. Geophys., 23, 885–900, doi:10.5194/angeo-23-885-2005, 2005.

Daum, P., Denton, M. H., Wild, J. A., Taylor, M. G. G. T., Šafránková, J., and Hayosh, M.: A general Cluster data and global MHD simulation comparison, Ann. Geophys., 26, 3411–3428, doi:10.5194/angeo-26-3411-2008, 2008.

De Sterck, H., Low, B. C., and Poedts, S.: Complex magnetohydrodynamic bow shock topology in field-aligned low-β flow around a perfectly conducting cylinder, Phys. Plasmas, 5, 4015–4027, doi:10.1063/1.873124, 1998.

Dmitriev, A. V. and Suvorova, A. V.: Traveling magnetopause distortion related to a large-scale magnetosheath plasma jet: THEMIS and ground-based observations, J. Geophys. Res, 117, A08217, doi:10.1029/2011JA016861, 2012.

Farris, M. H. and Russell, C. T.: Determining the standoff distance of the bow shock: Mach number dependence and use of models, J. Geophys. Res., 99, 17681–17689, doi:10.1029/94JA01020, 1994.

Farris, M. H., Petrinec, S. M., and Russell, C. T.: The thickness of the magnetosheath: Constraints on the polytropic index, Geophys. Res. Lett., 18, 1821–1824, doi:10.1029/91GL02090, 1991.

Gosling, J. T., Skoug, R. M., McComas, D. J., and Smith, C. W.: Direct evidence for magnetic reconnection in the solar wind near 1 AU, J. Geophys. Res., 110, A01107, doi:10.1029/2004JA010809, 2005.

Hietala, H., Laitinen, T. V., Andréeová, K., Vainio, R., Vaivads, A., Palmroth, M., Pulkkinen, T. I., Koskinen, H. E. J., Lucek, E. A., and Rème, H.: Supermagnetosonic Jets behind a collisionless quasiparallel shock, Phys. Rev. Lett., 103, 245001, doi:10.1103/PhysRevLett.103.245001, 2009.

Hietala, H., Partamies, N., Laitinen, T. V., Clausen, L. B. N., Facskó, G., Vaivads, A., Koskinen, H. E. J., Dandouras, I., Rème, H., and Lucek, E. A.: Supermagnetosonic subsolar magnetosheath jets and their effects: from the solar wind to the ionospheric convection, Ann. Geophys., 30, 33–48, doi:10.5194/angeo-30-33-2012, 2012.

Kallio, E. J. and Koskinen, H. E. J.: A semiempirical magnetosheath model to analyze the solar wind-magnetosphere interaction, J. Geophys. Res., 105, 27469–27479, doi:10.1029/2000JA900086, 2000.

Karlsson, T., Brenning, N., Trotignon, J.-G., Vallières, and Facskó, G.: Localized density enhancements in the magnetosheath: Three-dimensional morphology and possible importance for impulsive penetration, J. Geophys. Res., 117, A03227, doi:10.1029/2011JA017059, 2012.

Lavraud, B. and Borovsky, J. E.: Altered solar wind-magnetosphere interaction at low Mach numbers: Coronal mass ejections, J. Geophys. Res., 113, A00B08, doi:10.1029/2008JA013192, 2008.

Lavraud, B., Borovsky, J. E., Ridley, A. J., Pogue, E. W., Thomsen, M. F., Rème, H., Fazakerly, A. N., and Lucek, E. A.: Strong bulk plasma acceleration in Earth's magnetosheath: A magnetic slingshot effect?, Geophys. Res. Lett., 34, L14102, doi:10.1029/2007GL030024, 2007.

Le, G., Gosling, J. T., Russell, C. T., Elphic, R. C., Thomsen, M. F., and Newbury, J. A.: The magnetic and plasma structure of flux transfer events, J. Geophys. Res., 104, 233–245, doi:10.1029/1998JA900023, 1999.

Lin, R., Anderson, K. A., Ashford, S., Carlson, C. W., Curtis, D., Ergun, R., Larson, D., McFadden, J. P., McCarthy, M., Parks, G. K., Rème, H. abd Bosqued, J. M., Coutelier, J., Cotin, F., D'Uston, C., Wenzel, K.-P., Sanderson, T. R., Henrion, J., Ronnet, J. C., and Paschmann, G.: A three-dimensional plasma and energetic particle investigation for the WIND spacecraft, Space Sci. Rev., 71, 125–153, doi:10.1007/BF00751328, 1995.

Lin, Y., Lee, L. C., and Yan, M.: Generation of dynamic pressure pulses downstream of the bow shock by variations in the interplanetary magnetic field orientation, J. Geophys. Res., 101, 479–493, doi:10.1029/95JA02985, 1996a.

Lin, Y., Swift, D. W., and Lee, L. C.: Simulation of pressure pulses in the bow shock and magnetosheath driven by variations in interplanetary magnetic field direction, J. Geophys. Res., 101, 27251–27269, doi:10.1029/96JA02733, 1996b.

Lucek, E. A., Constantinescu, D., Goldstein, M. L., Pickett, J., Pinçon, J. L., Sahraoui, F., Treumann, R. A., and Walker, S. N.: The Magnetosheath, Space Sci. Rev., 118, 95–152, doi:10.1007/s11214-005-3825-2, 2005.

Luhmann, J. G., Russell, C. T., and Elphic, R. C.: Spatial distributions of magnetic field fluctuations in the dayside magnetosheath, J. Geophys. Res., 91, 1711–1715, doi:10.1029/JA091iA02p01711, 1986.

McFadden, J. P., Carlson, C. W., Larson, D., Ludlam, M., Abiad, R., Elliott, B., Turin, P., Marckwordt, M., and Angelopoulos, V.: The THEMIS ESA Plasma Instrument and In-flight Calibration, Space Sci. Rev., 141, 277–302, doi:10.1007/s11214-008-9440-2, 2008a.

Němeček, Z., Šafránková, J., Přech, L., Sibeck, D. G., Kokubun, S., and Mukai, T.: Transient flux enhancements in the magnetosheath, Geophys. Res. Lett., 25, 1273, doi:10.1029/98GL50873, 1998.

Němeček, Z., Šafránková, J., Pišoft, P., and Zastenker, G. N.: Statistical study of ion flux fluctuations in the magnetosheath, Czech. J. Phys., 51, 853–862, doi:10.1023/A:1011630618180, 2001.

Paschmann, G., Sonnerup, B. U. ., Papamastorakis, I., Sckope, N., Haerendel, G., Bame, S. J., Asbridge, J. R., Gosling, J. T., Russell, C. T., and Elphic, R. C.: Plasma acceleration at the Earth's magnetopause: evidence for reconnection, Nature, 282, 243–246, doi:10.1038/282243a0, 1979.

Phan, T. D., Paschmann, G., Twitty, C., Mozer, F. S., Gosling, J. T., Eastwood, J. P., Øieroset, M., Rème, H., and Lucek, E. A.: Evidence for magnetic reconnection initiated in the magnetosheath, Geophys. Res. Lett., 34, L14104, doi:10.1029/2007GL030343, 2007.

Powell, K. G., Roe, P. L., Linde, T. J., Gombosi, T. I., and De Zeeuw, D. L.: A Solution-adaptive upwind scheme for Ideal Magnetohydrodynamics, J. Comput. Phys., 154, 284–309, doi:10.1006/jcph.1999.6299, 1999.

Russell, C. T. and Elphic, R. C.: Initial ISEE magnetometer results: Magnetopause observations, Space Sci. Rev., 22, 681–715, doi:10.1007/BF00212619, 1978.

Šafránková, J., Hayosh, M., Němeček, Z., and Přech, L.: Magnetosheath Investigations: Interball Contribution to the Topic, in: Multiscale processes in the Earth's magnetosphere: From Interball to Cluster, edited by: Sauvaud, J. A. and Němeček, Z., vol. 178 of NATO science series, series ii: mathematics, physics and chemistry, pp. 73–94, Springer, 2004.

Savin, S., Amata, E., Zelenyi, L., Budaev, V., Consolini, G., Treumann, R., Lucek, E. A., Safrankova, J., Nemecek, Z., Khotyaintsev, Y., Andre, M., Buechner, J., Alleyne, H., Song, P., Blecki, J., Rauch, J. L., Romanov, S., Klimov, S., and Skalsky, A.: High energy jets in the Earth's magnetosheath: implications for plasma dynamics and anomalous transport, JETP Letters, 87, 593, doi:10.1134/S0021364008110015, 2008.

Savin, S., Budaev, V., Zelenyi, L., Amata, E., Sibeck, D., Lutsenko, V., Borodkova, N., Zhang, H., Angelopoulos, V., Safrankova, J., Nemecek, Z., Blecki, J., Buechner, J., Kozak, L., Romanov, S., Skalsky, A., and Krasnoselsky, W.: Anomalous Interaction of a Plasma Flow with the Boundary Layers of a Geomagnetic Trap, JETP Letters, 93, 754–762, doi:10.1134/S0021364011120137, 2011.

Savin, S., Amata, E., Zelenyi, L., Lutsenko, V., Safrankova, J., Nemecek, Z., Borodkova, N., Buechner, J., Daly, P. W., Kronberg, E. A., Blecki, J., Budaev, V., Kozak, L., Skalsky, A., and Lezhen, L.: Super fast plasma streams as drivers of transient and anomalous magnetospheric dynamics, Ann. Geophys., 30, 1–7, doi:10.5194/angeo-30-1-2012, 2012.

Schwartz, S. J., Thomsen, M. F., Bame, S. J., and Stansberry, J.: Electron Heating and the Potential Jump Across Fast Mode Shocks, J. Geophys. Res., 93, 12923–12931, doi:10.1029/JA093iA11p12923, 1988.

Shue, J.-H., Song, P., Russell, C. T., Steinberg, J. T., Chao, J.-K., Zastenker, G., Vaisberg, O. L., Kokubun, S., Singer, H. J., Detman, T. R., and Kawano, H.: Magnetopause location under extreme solar wind conditions, J. Geophys. Res., 103, 17691–17700, doi:10.1029/98JA01103, 1998.

Shue, J.-H., Chao, J.-K., Song, P., McFadden, J. P., Suvorova, A., Angelopoulos, V., Glassmeier, K. H., and Plaschke, F.: Anomalous magnetosheath flows and distorted subsolar magnetopause for radial interplanetary magnetic fields, Geophys. Res. Lett., 36, L18112, doi:10.1029/2009GL039842, 2009.

Smith, E. J.: Identification of interplanetary tangential and rotational discontinuities, J. Geophys. Res., 78, 2054–2063, doi:10.1029/JA078i013p02054, 1973.

Smith, C. W., L'Heureux, J., Ness, N. F., Acuña, M. H., Burlaga, L. F., and Scheifele, J.: The ACE Magnetic fields experiment, Space Sci. Rev., 86, 613–632, doi:10.1023/A:1005092216668, 1998.

Torrence, C. and Compo, G. P.: A practical guide to wavelet analysis, B. Am. Meteorol. Soc., 79, 61–78, doi:10.1175/1520-0477(1998)079<0061:APGTWA>2.0.CO;2, 1998.

Tsubouchi, K. and Matsumoto, H.: Effect of upstream rotational field on the formation of magnetic depressions in a quasi-perpendicular shock downstream, J. Geophys. Res., 110, A04101, doi:10.1029/2004JA010818, 2005.

Vasquez, B. J., Abramenko, V. I., Haggerty, D. K., and Smith, C. W.: Numerous small magnetic field discontinuities of Bartels rotation 2286 and the potential role of Alfvénic turbulence, J. Geophys. Res., 112, A11102, doi:10.1029/2007JA012504, 2007.

Walén, C.: On the theory of sunspots, Ark. Mat. Astron. Fys., 30A, 1–87, 1944.